PCCP

Order–disorder in grossly non-stoichiometric $SrFeO_{2.50}$ — a simulation study†

Egil Bakken,[a] Neil L. Allan,[b] T. Hugh K. Barron,[b] Chris E. Mohn,[a] Ilian T. Todorov[b] and Svein Stølen*[a]

[a] *Department of Chemistry, University of Oslo, Postbox 1033 Blindern, N0315 Oslo, Norway. E-mail: svein.stolen@kjemi.uio.no; Fax: +47 22 85 54 41; Tel: +47 22 85 56 01*
[b] *University of Bristol, School of Chemistry, Cantock's Close, Bristol, UK BS8 1TS*

Received 6th January 2003, Accepted 6th February 2003
First published as an Advance Article on the web 17th February 2003

Configurational lattice energy techniques are used to investigate oxygen vacancy ordering and the order–disorder transition in $SrFeO_{2.50}$. Vacancy disorder is shown to present many new challenges, largely due to the extensive relaxation in such grossly non-stoichiometric systems. With large supercells it is not feasible to optimise each individual configuration. Efficient methods for choosing a small number of representative configurations are discussed. Oxygen vacancy–vacancy interactions are considerable in $SrFeO_{2.50}$ and lead to the formation of preferred local structural entities. While the low-temperature structure consists of an ordered arrangement of octahedra and tetrahedra, the disordered high-temperature structure may be described as a mixture of tetrahedra, square pyramids and octahedra. Fe atoms with coordination numbers lower than four are negligible. The assumption of an ideal solution of oxygen vacancies in such systems, commonly made in standard thermodynamic treatments, is questionable.

1. Introduction

The energetics of grossly disordered materials remains poorly understood and in particular energetic contributions of configurational origin are difficult to assess. Whilst random distribution-type approximations appear to be appropriate in systems with weakly interacting defects, defects that interact strongly result in pronounced short-range order that is far from straightforward to treat mathematically.

Consider, for example, a perovskite-type oxide ABO_3. When reduced, forming $ABO_{3-\delta}$, some of the oxygen sites are vacant. It is commonly assumed that there is a completely random distribution of these vacancies over the oxygen sublattice. This assumption of ideality in turn implies a finite probability that a B-atom is surrounded by five or six anion vacancies. Chemical intuition suggests this is likely to be energetically highly unfavourable. The likely importance of short-range order is suggested by the common formation of ordered structures by perovskite-type oxides at low temperatures. In these, the B-atom, often a transition metal, is coordinated to six (octahedral), five (square pyramidal) or four (tetrahedral or square planar) oxygen atoms. Examples are the ordered arrangement of 50% octahedra and 50% square planar structural entities in $La_2Ni_2O_5$,[1] of 50% octahedral and 50% tetrahedra in $Ca_2Fe_2O_5$[2] and of 100% square pyramids in $Sr_2Mn_2O_5$.[3] Often only one type of "reduced" polyhedron is observed in a given compound, at least at low temperatures. There must therefore be an energetic preference for the polyhedron adopted by a given metal atom in a particular compound. The magnitude of this enthalpic term is not known. In some oxides a mixture of polyhedra is observed, indicating that the enthalpy difference between different orderings is not too large; in $La_{8-x}Sr_xCu_8O_{20}$, for example, CuO_6 octahedra, CuO_5 square pyramids and CuO_4 square planar entities are all observed.[4] On heating, changes in structure take place and phase transitions to disordered modifications are often observed. Nevertheless, a significant degree of short-range order may still be present even in disordered high-temperature states. In the present paper we investigate the effects of oxygen ordering and the formation of favoured structural entities on the structural and thermodynamic properties of grossly non-stoichiometric oxides, through a series of lattice energy calculations.[5]

We take as our model system $SrFeO_{3-\delta}$ ($0 \leq \delta \leq 0.5$), which is grossly non-stoichiometric at high temperatures. We have studied this system thoroughly[6–8] as part of a larger investigation on the energetics of grossly non-stoichiometric oxides.[9] Strong defect–defect interactions give rise to three reduced, vacancy-ordered, low-symmetry phases on cooling: $Sr_8Fe_8O_{23}$ (or $SrFeO_{2.875}$), $Sr_4Fe_4O_{11}$ (or $SrFeO_{2.75}$), and $Sr_2Fe_2O_5$ (or $SrFeO_{2.5}$).[10] We pay particular attention to the structural order–disorder transition[10,11] in $SrFeO_{2.5}$, which at low temperatures adopts the ordered brownmillerite-type structure,[10–12] with half the Fe(III) occupying octahedral sites and the remainder tetrahedral sites, and at 1120 K transforms discontinuously to disordered perovskite-type $SrFeO_{2.5}$.[6,10,13]

Grossly non-stoichiometric compounds in general and oxygen-deficient ceramics are particularly challenging for theory. Previous studies of grossly disordered systems have been largely restricted to systems with weak defect–defect interactions, such as solid solutions where the disorder is confined to the cation lattice with modest deviations from ideality.[14,15] Our long term aim is a quantitatively accurate description of a wide range of specific systems. This present study focuses on the underlying methods, but also provides a picture of the short-range order present in grossly non-stoichiometric oxides such as $SrFeO_{2.5}$.

We have recently been developing a number of new general techniques[16,17] for simulating *grossly-nonstoichoimetric* solids

† Presented at the 78th International Bunsen Discussion Meeting on "Complex Oxides: Defect Chemistry, Transport and Chemical Reaction", Vaals, The Netherlands, October 6–9, 2002.

This journal is © The Owner Societies 2003

and *solid solutions*. A key feature of all these is to sample many different configurations, allowing the exchange of ions or vacancies located at crystallographically inequivalent positions. Any method must also take into account the local environment of each ion, and in particular the structural and thus energetic relaxation which accompany an exchange of ions. Ion association and clustering must not be averaged out.

Configurationally averaged lattice dynamics involves the evaluation of an appropriate thermodynamic average over a (limited) set of calculations, each representing different arrangements or configurations of the cations within a supercell.[16] The accurate calculation of the enthalpy in the static limit of each configuration is quick and computationally efficient. In each configuration the energy is minimised with respect to the unit-cell dimensions and the atomic positions.[18] When the Gibbs energy of each configuration is minimised with respect to all structural variables, the resulting entropy includes *both* configurational *and* vibrational contributions. In the present work we neglect the vibrational contribution and minimise only the enthalpy in the static limit; this gives the configurational entropy that is the major contribution to the entropy increase accompanying the order–disorder transition. No *a priori* assumptions are made regarding this contribution. Applications to mixing properties of solid solutions of binary oxides using this technique are presented elsewhere.[14,15,19] We shall see that vacancy disorder produces many new challenges, largely due to the extensive relaxation which accompanies vacancy motion and the formation of preferred local structural entities in systems such as $SrFeO_{2.5}$.

2. Methods

The success of any atomistic simulation relies on the accuracy and transferability of the short-range interatomic potentials. All calculations are based on an ionic model using two-body potentials to represent short-range forces and the Ewald summation used for the long-range Coloumbic interactions. A conventional Born model is used, assigning integral ionic charges, based on accepted chemical valence rules, to all species (*i.e.* 2+ to Sr, 3+ or 4+ to Fe and 2− to O). Cation–oxygen interactions were described by a set of 2-body interionic potentials of the form $A\exp(-r/\rho)$, where the constants A and ρ are listed in Table 1 and r is the interionic distance. Oxide ion polarisability was taken into account by using the shell model of Dick and Overhauser,[20] and the shell charge and spring constant are also given in Table 1. This set of potentials was developed to reproduce closely the lattice parameters and average iron–oxygen bond lengths of the ordered low temperature orthorhombic form of $SrFeO_{2.5}$ ($Sr_2Fe_2O_5$), as shown in Table 2 where we compare experimental and simulated structural data for this phase. The same potentials are used unchanged for the high temperature phase. The non-Coulombic interatomic potential for Fe^{4+} used for a small number of defect calculations in the dilute limit (*i.e.* point defects in $SrFeO_3$) is also given in Table 1, and was obtained by fitting to reproduce the lattice parameter of the cubic perovskite $SrFeO_3$. To check the model, bond lengths were calculated for $SrFeO_3$ and the intermediate compounds $Sr_4Fe_4O_{11}$ and $Sr_8Fe_8O_{23}$, together with lattice parameters for the intermediate compounds. These are compared with experimental data in Table 2.

Table 1 Non-Coulombic interatomic potential parameters for the $SrFeO_{2.50}$–$SrFeO_{3.00}$ system. Potentials are of the form $A\exp(-r/\rho)$. The cut-off distance for all potentials is 14 Å. The shell charge on oxygen was $-2.5e$ and the associated spring constant 27 eV Å^{-2}

Interaction	A/eV	ρ/Å
Fe(III)/O^{2-}	3358.400	0.2650
Fe(IV)/O^{2-}	4058.400	0.2650
Sr^{2+}/O^{2-}	3220.0	0.3067
O^{2-}/O^{2-}	249.3764	0.3621

Table 2 Crystal structure data for the ordered compounds; comparison of experimental data and simulation results. The final column (×2, ×1 *etc.*) lists the number of bonds with the given lengths

$Sr_2Fe_2O_5$	Observed[12]	Calculated	Deviation	
a/Å	5.672(1)	5.746	1.5%[a]	
b/Å	15.59(2)	15.219	−2.4%[a]	
c/Å	5.527(1)	5.589	1.1%[a]	
V/Å^3	488.73	488.76	0.1%	
Octahedral Fe(1) site, Fe(III)				
Fe(1)–O(1)/Å	1.870	2.002		×2
Fe(1)–O(2)/Å	2.083	2.015		×2
Fe(1)–O(3)/Å	2.162	2.136		×2
Average	2.041	2.051	0.5%	
Tetrahedral Fe(2) site, Fe(III)				
Fe(2)–O(1)/Å	1.867	1.881		×1
Fe(2)–O(2)/Å	1.932	1.871		×2
Fe(2)–O(3)/Å	1.906	1.881		×1
Average	1.909	1.876	−1.7%	
$Sr_4Fe_4O_{11}$	Observed[12]	Calculated	Deviation	
a/Å	10.974(1)	10.867	−1.9%	
b/Å	7.702(1)	7.866	2.1%	
c/Å	5.473(1)	5.424	−0.9%	
V/Å^3	462.59(18)	463.64	0.2%	
Square-pyramidal Fe(1) site, Fe(III)				
Fe(1)$^{3+}$–O(1)/Å	1.902	1.788		×1
Fe(1)$^{3+}$–O(3)/Å	1.855	1.946		×4
Average	1.864	1.914	2.7%	
Octahedral Fe(2) site, Fe(IV)				
Fe(2)–O(2)/Å	1.937	1.966		×2
Fe(2)–O(3)/Å	2.044	1.939		×4
Average	2.008	1.948	−3.0%	
$Sr_8Fe_8O_{23}$	Observed[12]	Calculated	Deviation	
a/Å	10.929(1)	10.874	−0.5%	
c/Å	7.698(1)	7.777	1.0%	
V/Å^3	919.47	919.56	0.0%	
Square-pyramidal Fe(1) site, Fe(III)				
Fe(1)–O(1)/Å	1.926	1.814		×1
Fe(1)–O(2)/Å	1.851	1.944		×4
Average	1.866	1.918	2.8%	
Octahedral Fe(2) site, Fe(IV)				
Fe(2)–O(2)/Å	2.036	1.925		×2
Fe(2)–O(3)/Å	1.931	1.937		×2
Fe(2)–O(4)/Å	1.952	1.950		×2
Average	1.973	1.937	−1.8%	
Octahedral Fe(3) site, Fe(IV)				
Fe(3)–O(4)/Å	1.912	1.919		×4
Fe(3)–O(5)/Å	1.925	1.944		×2
Average	1.921	1.927	0.3%	
Sr_2FeO_3	Observed[12]	Calculated	Deviation	
a/Å	3.851(1)	3.850	0.0%[a]	
Octahedral Fe(1) site, Fe(IV)				
Fe(1)–O(1)/Å	1.926	1.925	−0.1%	×6

[a] Value used in fitting.

2.1. Defect energies at infinite dilution (point defects)

We also calculate a small number of *point-defect* internal energies at constant volume in the dilute limit, using the conventional two-region approach.[5] In this method the total energy of the defective system is minimised by a relaxation of the nuclear positions and shell displacements of the ions surrounding the defect. It is a reasonable assumption that this relaxation is greatest in the proximity of the defect and decreases fairly rapidly with distance away from the defect. The crystal is accordingly partitioned into a region immediately surrounding the defect, where the relaxations are assumed to be greatest, and an outer region that is only slightly perturbed. In the inner region the appropriate elastic equations for the force are solved explicitly, yielding the relaxed nuclear positions and shell displacements. Relaxation in the outer region is estimated using a suitable approximation due to Mott and Littleton.[21] In our calculations the inner region typically contained about 200 ions. The program GULP[22] was used in all calculations.

2.2. Defects energies in grossly disordered materials

Our method for grossly nonstoichiometric oxides employs the full structural optimisation of periodic systems with large unit cells, by means of a combination of lattice statics and quasi-harmonic lattice dynamics. An appropriate thermodynamic average over a set of calculations is evaluated for different configurations of vacancies within a supercell, using methods discussed previously.[14–16]

Given the Gibbs energy, G_k, for the *relaxed* (optimised) structure of each possible configuration k we then average:

$$H = \frac{\sum_{k}^{K} H_k \exp(-G_k/k_B T)}{\sum_{k=1}^{K} \exp(-G_k/k_B T)}, \quad (1)$$

$$G = -k_B T \ln \sum_{k=1}^{K} \exp(-G_k/k_B T), \quad (2)$$

$$S = \frac{H}{T} + k_B \ln(\sum_{k=1}^{K} \exp(-G_k/k_B T)) \quad (3)$$

where K is the total number of possible configurations for the supercell considered. Here K equals $N!/[N_V!N_O!]$ where N is the total number of oxygen sites and N_O and N_V the number of oxygen atoms and oxygen vacancies in a particular supercell.

In previous work[15,16,19] eqns. (1)–(3) were used to study solid solutions of binary oxides and each arrangement k represented a different configuration of cations. For any but the smallest cell sizes it was not possible to sum over all possible configurations. In these studies the solutions were close to ideal and K' particular arrangements were chosen entirely at random. These K' arrangements were then used in the evaluation of eqns. (1)–(3). In eqn. (1) the sum is simply restricted to K' rather than K arrangements. Eqn. (2) becomes

$$G = -k_B T \ln\left(\sum_{k=1}^{k=K'} \left(\frac{K}{K'}\right) \exp(-G_k/k_B T)\right)$$
$$= -k_B T \ln K - k_B T \ln\left(\sum_{k=1}^{k=K'} \left(\frac{1}{K'}\right) \exp(-G_k/k_B T)\right) \quad (4)$$

Eqn. (4) thus assumes that all the K' configurations that are chosen at random have the same degeneracy, K/K'. For systems such as $SrFeO_{2.50}$ with strong defect–defect interactions a random choice of configurations may be poor.

In this paper we ignore vibrational contributions to the Gibbs energy G_k of each configuration. The vibrational entropy and the vibrational contribution to the enthalpy is neglected and the energy of each configuration is generated in the static limit ($G_k = H_k^{static}$). The program GULP was used for all such structural optimisations.[22] Entropies calculated using the resulting values thus represent solely the *configurational* contribution to the total entropy of the system.

3. Results and discussion

3.1. Defects at infinite dilution

Conventional thermodynamic models for the entropy of oxygen-deficient perovskites and indeed oxygen vacancy disorder more generally, use expressions assuming ideal behaviour on the oxygen sublattice. Since the effective charge of an oxygen vacancy is 2+, this is unlikely to be a good approximation. To illustrate this point, we have carried out a set of model point-defect calculations for the end-member compound $SrFeO_3$.

An increasing number of oxygen vacancies are successively introduced into the octahedron of oxygen ions which surround a specific Fe atom. Fig. 1 displays the defect energies *per vacancy* as a function of the total number of vacancies in the octahedron, and shows that in the dilute limit it becomes steadily more expensive to introduce an additional vacancy into a polyhedron where one or more vacancies are already present. There is a strong repulsive interaction between vacancies. When two vacancies are introduced these may be located either on opposite sides or on the same face of the FeO_6 octahedron. The latter is the most favourable in our example, where relaxation leads to a local tetrahedral rather than square planar geometry. This illustrates the role that is played by the elastic forces in addition to the effective charges of the defects, which by themselves would favour the square planar rather than tetrahedral geometry. In addition, attempts to place more than three oxygen vacancies in the same octahedron fail, because during relaxation oxygen atoms migrate from surrounding octahedra and increase the coordination number of the Fe defect centre. All such physically unrealistic configurations are nevertheless assumed to be possible in an ideal solution model. The assumption of ideality is thus unjustified. In the next section we move on to the details of a model in which defect–defect interactions are explicitly accounted for and the calculations are *not* confined to the dilute limit.

3.2. Simulations of grossly disordered materials with strong defect–defect interactions

$SrFeO_{2.5}$ is a complex system from a computational point of view. We neglect any configurational disorder in the low

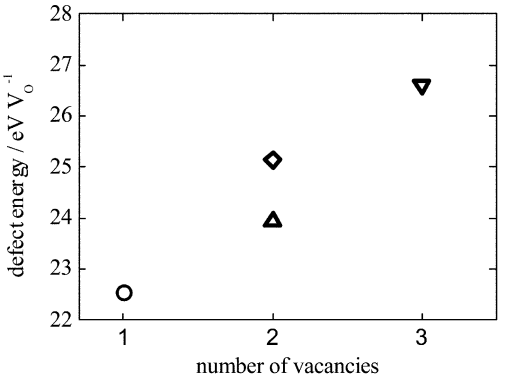

Fig. 1 The defect internal energy per oxygen vacancy in $SrFeO_{3.0}$ as a function of the total number of vacancies in the octahedron. ○, △, ◇, and ▽ represent square pyramidal, tetrahedral, square planar and triangular local arrangement of the remaining oxygen atoms around the central Fe-ion.

temperature orthorhombic brownmillerite phase,[13] and vibrational contributions are also ignored. With these assumptions the Gibbs energy of this phase is equal to the enthalpy in the static limit.

For the high temperature disordered phase of $SrFeO_{2.5}$ we start with a cubic perovskite supercell containing 40 atoms. We generate initial configurations by removing the appropriate number of oxygen atoms from the 'undefective' structure $SrFeO_3$. One-sixth of the oxygen sites occupied in this end-member compound are empty. We then estimate the enthalpy and configurational entropy of this phase using configurational averaging (eqns. (1)–(3)). Individual configurations are not constrained to retain cubic symmetry during the optimisations. Note that this choice of supercell does not permit the formation of the low temperature phase.

The interactions between the vacancies are large, and it is not clear how many configurations should be included in the summations in eqns. (1)–(3). If a purely random subset of configurations is chosen there is a clear danger that important low-energy configurations will be omitted. In our $2 \times 2 \times 2$ cubic cell for $SrFeO_{2.50}$ there are 20 oxygen atoms distributed over 24 possible sites. This gives a total of 10 626 configurations even for such a small cell. Nevertheless, given the computational efficiency of the structural optimisation, within the pair-potential model, it is possible to optimise *all* these configurations. Eqns. (1)–(3) can then be used directly to obtain the thermodynamic properties for the disordered phase. An advantage is that the consequences of using only a subset of configurations can then also be assessed.

We have optimised all 10 626 configurations in the static limit. For many configurations and especially those high in energy‡ this proved to be a far from trivial task. The relaxation of the structure around the oxygen vacancies is extensive—much more so than in the solid solutions containing two different cations that we have considered previously using configurational averaging. Large structural reconstructions such as the formation of a tetrahedron from the initial geometrical arrangement formed by the removal of one equatorial and one apical oxygen atom from a FeO_6 octahedron often converged slowly. Problems also arose due to the tendency of oxygen atoms to migrate from one coordination sphere to another. A second order optimisation method (Hessian update at every iteration)[22] with a step size of 0.3 was used. It proved helpful to vary the initial volume of the supercell in a systematic manner in order to achieve convergence of the different configurations. As an example Fig. 2 shows the norm of the energy gradient (implemented in GULP as the sum of the gradients of all variables squared, divided by the number of variables[22]) as a function of the number of optimisation iterations for a 'well-behaved' configuration and for a 'problem' configuration. During the optimisation of the 'problem' configuration the norm of the gradient passes through two minima and the total number of iterations necessary for an apparently successful optimisation is large. The energy surface is flat which facilitates migration of oxygen atoms and/or vacancies and thus changes in the coordination number of specific iron atoms from those in the initial configuration. We define somewhat arbitrarily the radius of the first coordination sphere around a Fe atom to be 2.9 Å, which is about 1 Å longer than a typical Fe(III)–O bond length. The problem configuration of Fig. 2 corresponds to one in which the coordination number has changed at the end of the optimisation. In such cases the energy of a given "problem" configuration is assigned from the plots as the energy which corresponds to the last minimum in the norm of the gradient whilst retaining the initial Fe coordination number. The facile oxygen migration in perovskite-type systems at higher temperatures is well known and there are

‡ Since we work at zero pressure throughout, all energies in this and later sections are strictly enthalpies.

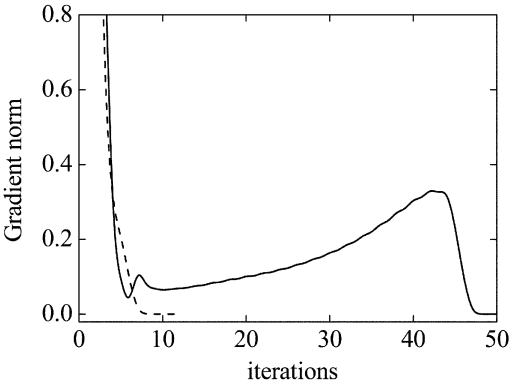

Fig. 2 The norm of the energy gradient as a function of the number of optimisation iterations for a "well-behaved" configuration (dashed line) and for a "problem" configuration (solid line). See text for further explanation.

several good oxygen ion conductors of composition $ABO_{2.5}$, *e.g.* $Ba_2In_2O_5$,[23,24] known. High ionic conductivity is consistent with the oxygen diffusion coefficient obtained from a short series of molecular dynamics simulations on a number of configurations at 1500 K, using the same set of potentials as here.[25]

Using all 10 626 configurations to calculate the Gibbs energy of the disordered cubic phase *via* eqn. (2) and comparing this with the energy of the ordered brownmillerite structure leads to a calculated phase transition at $T_{trs} \approx 3500$ K. While this is acceptable for such a simple model, it is still markedly higher than the observed transition temperature (1120 K). There are a number of possible reasons for this discrepancy. Most importantly, the supercell is still relatively small. In addition to the effect of periodic symmetry on the energies, the degeneracies of low-lying excited states will be greater in a larger cell. Thermal expansion, which would be expected to assist the orthorhombic–cubic transition by enabling mutual rotation of the FeO_6 octahedra, is ignored. The potential model is also relatively crude; the difference between k_BT at 1120 K and 3500 K is only $\approx$20 kJ mol^{-1}. The discrepancy is relatively unimportant for our present purpose of examining a suitable model system.

The variation of the entropy with temperature for the low- and high-temperature phases is shown in Fig. 3. Note however that the entropy in the disordered phases is well below the ideal limit; it is only 93% of the ideal value for a $2 \times 2 \times 2$ cell even at $T/T_{trs} = 2.5$, where the system still shows a significant degree of vacancy ordering. We have therefore examined in detail the local structures of the various configurations of the disordered

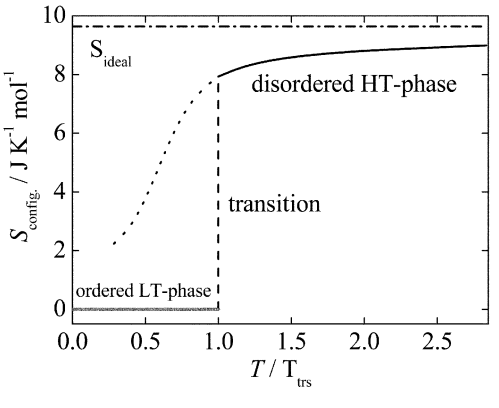

Fig. 3 Configurational entropy of $SrFeO_{2.50}$ as a function of T/T_{trs} for a $2 \times 2 \times 2$ cell. The dotted line shows the configurational entropy of the disordered modification at metastable conditions.

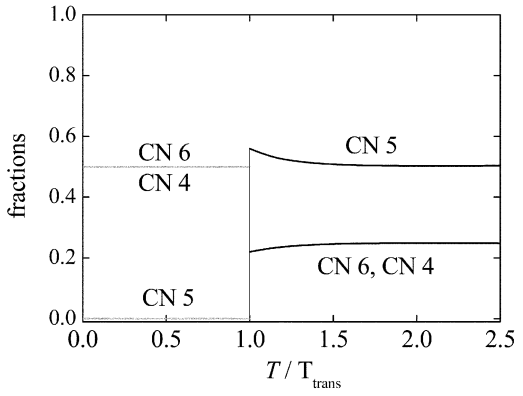

Fig. 4 Fraction of four (CN 4), five (CN 5) and six (CN 6)-coordinate Fe atoms in $SrFeO_{2.50}$ as a function of T/T_{trs} for a $2 \times 2 \times 2$ cell. The grey lines represent the ordered low-temperature phase, the solid lines the disordered high-temperature modification.

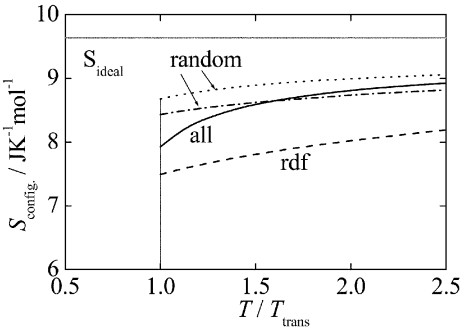

Fig. 5 Configurational entropy of disordered $SrFeO_{2.50}$ as a function of T/T_{trs} for a $2 \times 2 \times 2$ cell. The solid and dashed lines show results obtained using the symmetry and rdf-generators and the appropriate degeneracy of each generator. The remaining two curves represent values obtained using eqn. (4) and 10 configurations selected at random.

phase. The information gained is summarized in Fig. 4, where we plot the fraction of four, five and six-coordinate Fe atoms as a function of temperature. Low energy configurations of the cubic phase, *i.e.* those significant at the transition temperature, contain a mixture of octahedra (six-coordinate Fe), square pyramids (five-coordinate Fe) and tetrahedra (four-coordinate Fe). Configurations containing lower-coordinate Fe or square planar FeO_4 entities are much higher in energy. The low temperature brownmillerite orthorhombic phase contains an ordered arrangement of octahedra and tetrahedra; the high temperature phase is largely comprised of the same units plus square pyramids but in a more random arrangement. A useful picture of the disorder, preferable to that of a random arrangement of oxygen vacancies, is thus one involving a distribution of structural entities—octahedra, tetrahedra and square pyramids. The probabilities of octahedral, tetrahedral/square planar entities and square pyramids for a purely a random distribution of vacancies on the oxygen sub-lattice is 33.5, 20.1 and 40.2%. The simulations thus indicate that there is an increased probability for finding coordination numbers of 5 and 4 for the disordered modification when defect–defect energetics are taken into account. The importance of defect–defect interactions is clear.

3.3. Larger supercells and rdf-generators

With larger supercells it is not feasible to optimise each individual configuration. For example, for a $4 \times 4 \times 4$ cell the total number of configurations is 3×10^{36} and it will only be possible to optimise a small fraction of the total number. Also explicit optimisation of even as small a number as 10,000 configurations is an operation that will be very CPU-expensive for so large a cell as $4 \times 4 \times 4$. Methods for choosing a small number of low energy configurations are required, which can be tested against the results for the $2 \times 2 \times 2$ cell.

The simplest approach is to select a small number of randomly selected configurations for use in eqn. (4). Fig. 5 shows two calculations for the $2 \times 2 \times 2$ cell using different random sets of only 10 out of the total 10 626 configurations. Both sets give transition temperatures and entropies similar to those obtained from the full number of configurations. The transition temperatures differ by typically 10%, and the configurational entropy of the cubic disordered phase at $T/T_{trs} = 2.5$ differ by 2%. Still, the random sets miss the fall in the entropy with decreasing T of the high temperature phase (close to T_{trs}) as the low energy configurations are preferentially occupied. Even more importantly, the structural information obtained from such a small number of random configurations is inadequate, as shown in Fig. 6. The choice of configurations is thus crucial for the representation of the disordered structure and for larger supercells more efficient schemes are needed.

Evidently many configurations are related by symmetry, so we need only to evaluate the number of crystallographically distinct configurations and their associated degeneracies. We refer to these distinct configurations as 'generators'. For our $2 \times 2 \times 2$ supercell, symmetry reduces the 10 626 configurations to 78 generators. The energy *vs.* degeneracy for the $2 \times 2 \times 2$ cell is given in Fig. 7, where each open circle refers to a separate generator (some overlapping). This reduction from 10 626 to 78 gives a reduction in CPU time by over two orders of magnitude. However, we need to develop a computational method for the derivation of generators and their degeneracies before this can be done for larger cells.

We have therefore investigated a simpler, approximate, scheme based on the calculation of the V_O–V_O radial distribution function (rdf) of the cubic input geometry for each configuration, obtained by removing oxygen atoms from stoichiometric $SrFeO_3$. We refer to a set of initial configurations all with the same radial distribution function as an *rdf-generator*. The number of such rdf-generators, each with an associated degeneracy, is readily obtained; for the $2 \times 2 \times 2$ cell there are 38 rdf-generators.§ All configurations that belong to the same symmetry generator thus have the same rdf, but an rdf-generator may contain non-equivalent symmetry-generators which will, in general, lead to different final energies. The energies and degeneracies of the 38 rdf-generators are shown in Fig. 8.

Our approximation is to take just one configuration chosen at random from each of the 38 rdf-generators. The entropy and the fraction of the different structural entities obtained from these configurations and the associated degeneracy of each generator are given by dashed lines in Figs. 5 and 6. The energetic and structural properties are reproduced rather well, and relatively little thermodynamic or structural information is lost.

In order to see if a similar method can be used with larger super cells, we have tested a simplified approach. Again, we take one configuration at random to represent each rdf-generator and the same initial volume is used at the start of each minimisation; but now only the configurations that converge readily, with their associated degeneracies, are used in the thermodynamic averaging (so that eqn. (4) is used with K' equal to the sum of the degeneracies of the rdf-generators used). The entropy and fractions of square pyramids and

§ Alternatively, for our particular case, where the defects (the oxygen vacancies) have charge different from that of the host ions, the degeneracy of the rdf-generator is (within a pair-potential model) found by grouping together configurations with the same *initial* energy.

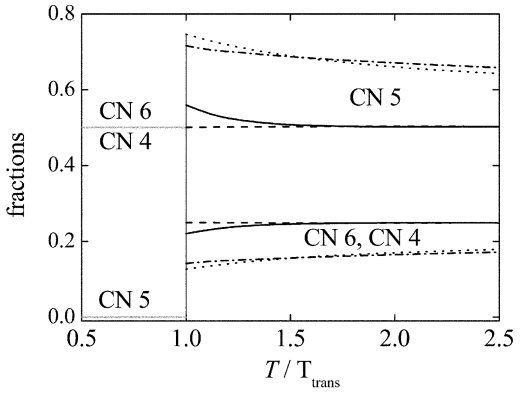

Fig. 6 Fraction of four (CN 4), five (CN 5) and six (CN 6)-coordinate Fe atoms in $SrFeO_{2.50}$ as a function of T/T_{trs}. The solid and dashed lines show results obtained using the symmetry and rdf-generators and the appropriate degeneracy of each generator. The remaining two curves represent values obtained using eqn. (4) and 10 configurations selected at random.

four-coordinate Fe at $T/T_{trs} = 2.5$ are then given as 8.2 J K^{-1} mol^{-1}, 0.497 and 0.251% respectively, compared to values of 8.9 J K^{-1} mol^{-1}, 0.503 and 0.248% obtained using all 10 626 configurations.

Since this simplified approach works well for the $2 \times 2 \times 2$ cell, we have in a preliminary study applied the same rdf-method to a somewhat larger supercell. For a $2 \times 2 \times 3$ supercell, with $\approx 2 \times 10^6$ configurations in total, the total number of rdf-generators is 5830. Configurations from many of these gave migrating oxygen atoms and thus change in the coordination numbers during optimization. After these were discarded, approximately 2000 *rdf*-configurations remained, all of which converged rapidly without changes in the coordination numbers. This gave results, which can be compared with those obtained for the $2 \times 2 \times 2$ cell. The presence of a relatively greater proportion of lower-energy configurations reduces the transition temperature to 1720 K, and the enthalpy and entropy of the transition are also reduced. The configurational entropy (again at $T/T_{trs} = 2.5$) as a percentage of the ideal value is reduced from 85% for the rdf-generators and the $2 \times 2 \times 2$ cell to 75% for the $2 \times 2 \times 3$ cell, while the fractional occurrence of square pyramids and four-coordinate Fe changes from 0.50 and 0.25 to approximately 0.40 and 0.30. The qualitative picture is unchanged. Further work is required here with substantially larger cell sizes, so as to obtain detailed quantitative information as well as largely qualitative insight.

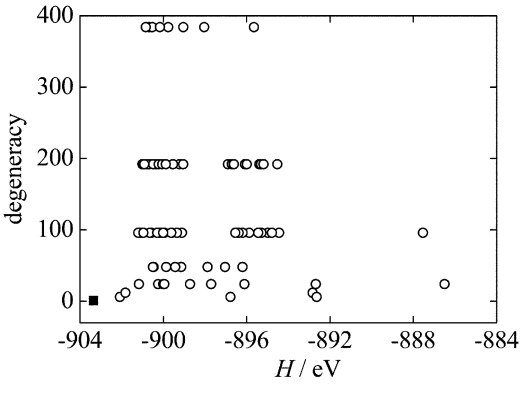

Fig. 7 Degeneracy *versus* relaxed enthalpy for the 78 symmetry generators that represent all 10 626 configurations of the $2 \times 2 \times 2$ super cell of $SrFeO_{2.50}$. Each open circle refers to a separate generator (some are overlapping).

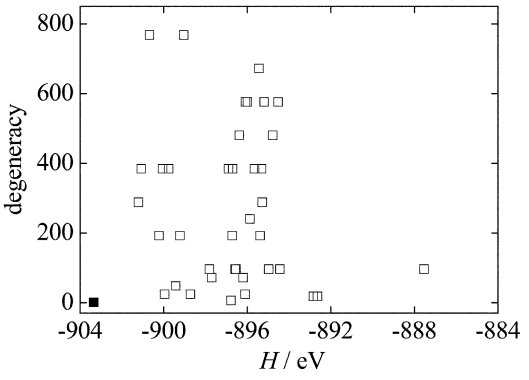

Fig. 8 Degeneracy *versus* relaxed enthalpy for the 38 rdf-generators for the $2 \times 2 \times 2$ super cell of $SrFeO_{2.50}$ optimising one configuration from each set of rdf's. Note that all configurations that belong to the same symmetry generator (shown in Fig. 7) have the same rdf, but an rdf-generator may contain non-equivalent symmetry-generators which will, in general, lead to different final energies.

3.4. Structural and energetic aspects of the order–disorder transition in $SrFeO_{2.50}$

Despite the crudity of the model, the entropy of transition (6.0 J K^{-1} mol^{-1} for the $2 \times 2 \times 3$ cell) is in good agreement with two recent experimental determinations (6.7[13] and 7.6 ± 1.2[6] J K^{-1} mol^{-1}). The entropy associated with the transition for the $2 \times 2 \times 2$ cell is much closer to its maximum possible value since there is a smaller number of configurations where more than 2 vacancies in an octahedron is possible here than for the larger cell. The negative volume change (−0.3%) observed experimentally[13] was reproduced in the simulations using the $2 \times 2 \times 2$ cell (−0.3%) while the volume change was close to zero for the limited number of configurations treated for the $2 \times 2 \times 3$ cell. As we have seen, the ordered low temperature phase consists of 50% octahedra and 50% tetrahedra while in the high-temperature phase the fraction of five-coordinated iron atoms is large. The decrease in the number of six-coordinate Fe ions with temperature is equal to that for four-coordinate Fe, since the dominant generating process involves the simultaneous transformation of one octahedron and one tetrahedron into two square pyramids and the number of two- and three-coordinate Fe atoms is negligible. Configurations with octahedra containing three or more oxygen vacancies are high in energy and do not contribute to the energetics except at the highest temperatures studied. Most of the four-coordinate Fe is tetrahedral rather than square planar at T_{trs}. The fraction of square planar entities increases at higher temperatures. It is worth stressing that in the dilute limit two Fe ions with coordination number five have a lower energy than one with four and one with six (see Fig. 1).

While the local symmetries of selected low energy configurations are quite high, as shown in Fig. 9 for octahedral, square pyramidal and tetrahedral environments, some entities present in higher energy configurations are less symmetric. The average Fe–O bond length and angles for selected entities

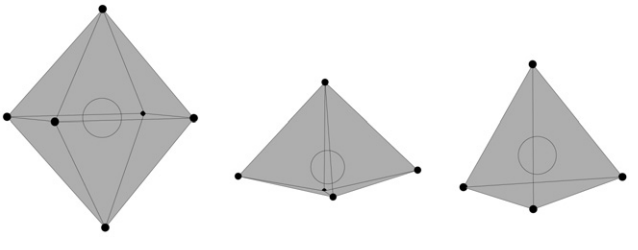

Fig. 9 Local symmetries of selected low energy configurations for octahedral, square pyramidal and tetrahedral environments.

Table 3 Local structure of structural entities in selected low and intermediate energy configurations. Experimental data from ref. 13 for the low-temperature modification at 1148 K are included for comparison. Average values and standard deviation are given

Entity	$H_{config.}$/eV	O–Fe–O angle/°	Fe–O distance/Å
Octahedra	−901.07	90 ± 4	2.1 ± 0.3
	−900.47	90 ± 4	2.04 ± 0.08
Expt.[13]		90 ± 2	2.1 ± 0.1
Square pyramids	−901.07	94 ± 6	1.93 ± 0.06
	−901.82	95 ± 8	1.94 ± 0.05
Tetrahedra	−901.07	109 ± 9	1.85 ± 0.03
	−900.47	110 ± 16	1.85 ± 0.02
Expt.[13]		110 ± 14	1.88 ± 0.05

present in some different low and intermediate-energy configurations are given in Table 3. The structural entities are deformed to a significant degree even below the transition temperature. Experimental data for orthorhombic $SrFeO_{2.5}$ for $T = 1148$ K are given in Table 3, and the structure is significantly deformed even at room temperature. The calculated averaged data presented in this table are thus in good agreement with experiment.

4. Conclusions

In this paper we have considered oxygen vacancy disorder in a crystal far from the dilute limit. We have shown that defect–defect interactions are considerable and that the high-temperature structure of $SrFeO_{2.5}$ may be described as a disordered mixture of tetrahedra, square pyramids and octahedra. Fe atoms with coordination numbers lower than four are negligible. The assumption of an ideal solution of oxygen vacancies in such systems, commonly made in standard thermodynamic treatments, is questionable.

Such highly non-ideal disordered systems present many challenges for the methodology and there remains much to do. We have been restricted to small cell sizes, which has prevented us from obtaining an accurate transition temperature between the ordered low and disordered high temperature phases. Improvements in method, such as the automatic calculation of the weights of individual configurations *via* their symmetry properties and novel Monte Carlo techniques,[19] are under development. Mixed valence oxides pose additional challenges because of the mixture of formal oxidation states. We hope to obtain an alternative general description of the solid state chemistry of this and related systems in terms of a small number of structural entities such as octahedra, square pyramids and tetrahedra.

Acknowledgements

This work was funded by Norsk Forskningsråd (project number 132014/410 and 142995/432) and EPSRC grant GR/M53899. Computational facilities were made available through grants of computer time for the Program for Supercomputing, Norway and two HEFCE JREI awards.We should like to thank John Purton for carrying out the molecular dynamics runs and the British Council and Norsk Forskningsråd for funding a collaborative project. We would like to acknowledge Julian Gale for advice related to the use of the GULP program package.

References

1 J. A. Alonso and M. Martinez-Lope, *J. Chem. Soc., Dalton Trans.*, 1995, **17**, 2819.
2 J. Berggren, *Acta Chem. Scand.*, 1971, **25**, 3616.
3 V. Caignaert, N. Nguyen, M. Hervieu and B. Raveau, *Mater. Res. Bull.*, 1985, **20**, 479.
4 C. Er-Rakho, C. Michel and B. Raveau, *J. Solid State Chem.*, 1988, **73**, 514.
5 *E.g.*, C. R. A. Catlow and W. C. Mackrodt, *Computer Simulation of Solids*, ed. C. R. A. Catlow and W. C. Mackrodt, Springer-Verlag, Berling, 1982, pp. 3–20.
6 C. Haavik, T. Atake, H. Kawaji and S. Stølen, *Phys. Chem. Chem. Phys.*, 2001, **3**, 3863.
7 C. Haavik, T. Atake and S. Stølen, *Phys. Chem. Chem. Phys.*, 2002, **4**, 1082.
8 H. Evenrud and S. Stølen, *J. Therm. Anal. Calorim.*, 2002, **69**, 795.
9 E. Bakken, T. Norby and S. Stølen, *J. Mater. Chem.*, 2001, **12**, 317.
10 Y. Takeda, K. Kanno, T. Takada and O. Yamamoto, *J. Solid State Chem.*, 1986, **63**, 237.
11 J. C. Grenier, N. Ea, M. Pouchard and P. Hagenmuller, *J. Solid State Chem.*, 1985, **58**, 243.
12 J. P. Hodges, S. Short, J. D. Jorgensen, X. Xiong, B. Dabrowski, S. M. Mini and C. W. Kimball, *J. Solid State Chem.*, 2000, **151**, 190.
13 M. Schmidt and S. J. Campbell, *J. Solid State Chem.*, 2001, **156**, 292.
14 J. A. Purton, J. D. Blundy, M. B. Taylor, G. D. Barrera and N. L. Allan, *Chem. Commun.*, 1998, 627.
15 N. L. Allan, G. D. Barrera, M. Yu. Lavrentiev, I. T. Todorov and J. A. Purton, *J. Mater. Chem.*, 2001, **11**, 63.
16 N. L. Allan, G. D. Barrera, R. M. Fracchia, M. Yu. Lavrentiev, M. B. Taylor, I. T. Todorov and J. A. Purton, *Phys. Rev. B*, 2001, **63**, 94 203.
17 M. Yu. Lavrentiev, N. L. Allan, G. D. Barrera and J. A. Purton, *J. Phys. Chem. B*, 2001, **105**, 3594.
18 M. B. Taylor, G. D. Barrera, N. L. Allan and T. H. K. Barron, *Phys. Rev. B*, 1997, **56**, 14 380.
19 N. L. Allan, G. D. Barrera, J. A. Purton, C. E. Sims and M. B. Taylor, *Phys. Chem. Chem. Phys.*, 2000, **2**, 1099.
20 B. G. Dick and A. W. Overhauser, *Phys. Rev.*, 1958, **112**, 90.
21 N. F. Mott and M. J. Littleton, *Trans. Faraday Soc.*, 1938, **34**, 485.
22 J. Gale, *J. Chem. Soc., Faraday Trans.*, 1997, **93**, 629; see also J. Gale, GULP 1.3 user manual (http://www/ch.ic.ac.uk/gale/Research/gman13.html).
23 P. Berastegui, S. Hull, F. J. Garcia-Garcia and S. -G. Eriksson, *J. Solid State Chem.*, 2002, **164**, 119.
24 G. B. Zhang and D. M. Smyth, *Solid State Ionics*, 1995, **82**, 161.
25 J. A. Purton, private communication.